The Finite-Element Method for Modeling Circuits and Interconnects for Electronic Packaging

Anastasis C. Polycarpou, Panayiotis A. Tirkas, *Member, IEEE,* and Constantine A. Balanis, *Fellow, IEEE*

***Abstract*—A full-wave finite-element method (FEM) is formulated and applied in the analysis of practical electronic packaging circuits and interconnects. The method is used to calculate S-parameters of unshielded microwave components such as patch antennas, filters, spiral inductors, bridges, bond wires, and microstrip transitions through a via. Although only representative microwave passive circuits and interconnects are analyzed in this paper, the underlined formulation is applicable to structures of arbitrary geometrical complexities including microstrip and coplanar-waveguide transitions, multiple conducting vias and solder bumps, multiple striplines, and multilayer substrates. The accuracy of the finite-element formulation is extensively verified by calculating the respective S-parameters and comparing them with results obtained using the finite-difference time-domain (FDTD) method. Computational statistics for both methods are also discussed.**

***Index Terms*—Electronic packaging, finite-element method, interconnects, passive circuits.**

I. Introduction

RECENT advancements in monolithic-microwave integrated-circuit (MMIC) technology resulted in electronic packages of significantly smaller size and a larger number of printed interconnects on the motherboard. Accurate design and optimization of such high-speed high-density microwave circuits and interconnects becomes a major challenge when it comes to high performance and low cost. High-frequency operation is usually the main cause of strong coupling and interference among neighboring transmission lines, thereby affecting the overall electrical performance of the package. The presence of abrupt discontinuities, microstrip bends, bond wires, metallic bridges, and vertical conducting vias results in additional parasitic effects such as radiation and time delays. The major objective of current technology is the design of electronic packages that are optimized to minimize severe parasitic effects without necessarily increasing the cost or the complexity of the manufacturing process.

The existing high demand for the development of more accurate, versatile, and efficient numerical models which can be used in the design and characterization of microwave circuits mandates the implementation of full-wave techniques such as the finite-difference time-domain (FDTD) method [1], the spectral-domain approach (SDA) [2], and the finite-element method (FEM) [3]. The FDTD method is probably the most extensively used technique for the analysis of geometrically complex packaging structures. It was initially applied for the evaluation of frequency-dependent parameters of basic microstrip discontinuities [4], [5]. It was later successfully implemented in the analysis of more complex structures such as filters, microstrip transitions, bond wires, bridges, etc. [6], [7]. However, the main drawback of the method is that curved surfaces and nonrectangular volumes are usually modeled using a staircasing approach. The SDA technique is also very popular in the area of microwave-circuit analysis and design. Its main disadvantage though is that it can only handle metallizations in the same plane. Although the method can be extended to treat conducting transitions in the vertical plane [8], it still is restricted to specific types of geometries. On the contrary, the FEM is the most versatile and flexible numerical technique to be used in the analysis of geometrically complicated electronic packaging structures. The introduction of vector finite elements [9], the valuable contributions on absorbing-boundary conditions (ABC's) [10] and the effectiveness of sparse matrix iterative solvers, created a conducive environment for the evolution of the method in the area of computational electromagnetics. The FEM has been extensively used for scattering and radiation problems [11], waveguide propagation problems [12], and analysis of two-dimensional (2-D) MMIC structures [13], [14]. Recently, the method has been applied in the S-parameter evaluation of three-dimensional (3-D) MMIC's such as microstrip transitions, planar discontinuities, and conducting vias [15]–[17].

This paper formulates a full-wave analysis and implementation of the FEM to geometrically complex and practical microwave circuits and interconnects. Unlike previous work on the subject [15]–[17], a 2-D eigenvalue analysis [14] is applied at the input port in order to compute the field distribution of the dominant and higher order modes; the microwave circuit is then excited with the governing modal distribution. The eigenvalue analysis is also applied to the output port in order to calculate the frequency-dependent propagation constant and characteristic impedance of the transmission line. The dispersive propagation constant at the input and output ports is used in the implementation of the ABC's, whereas the characteristic impedance is used in the evaluation of the S-parameters. The current formulation is proven to be *efficient, flexible,* and extremely *accurate* in analyzing complex

Manuscript received January 20, 1997; revised July 1, 1997. This work was supported by the U.S. Army Research Office under Grant DAAL03-92-G-0262.

A. C. Polycarpou and C. A. Balanis are with the Department of Electrical Engineering, Telecommunications Research Center, Arizona State University, Tempe, AZ 85287-7206 USA.

P. A. Tirkas was with the Department of Electrical Engineering, Telecommunications Research Center, Arizona State University, Tempe, AZ 85287-7206 USA. He is now with Space Systems/Loral, Palo Alto, CA 94303 USA.

Publisher Item Identifier S 0018-9480(97)07399-7.

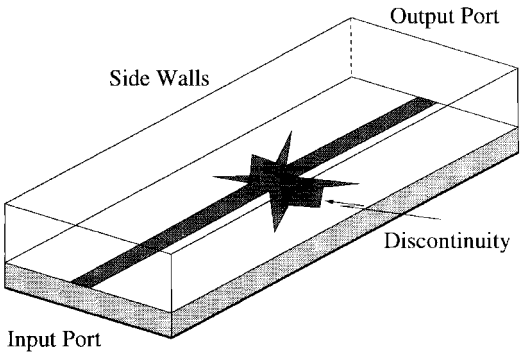

Fig. 1. 3-D rendering of a typical microstrip discontinuity.

microwave circuits and interconnects. It is *efficient* because of the use of a 2-D eigenvalue analysis to determine the excitation fields and needed circuit parameters. It is *versatile* because the input and output ports are not restricted to a single microstrip line—coplanar waveguides, coupled microstrip lines, and finlines can also be used. It is *accurate* because the excitation field, propagation constant, and characteristic impedance are computed at every frequency using a full-wave approach.

An outline of the FEM formulation used toward modeling complex microwave circuits and interconnects is provided in Section II. Similarly, a description of the FDTD implementation is given in Section III. Numerical results for several representative geometries including a microstrip patch antenna, a planar microwave filter, a circular spiral inductor connected in series or in parallel, and a package depicting a double-via transition between two microstrip lines are presented in Section IV. For some of these cases, a comparison between the FEM and FDTD method is shown.

II. The FEM

A full-wave FEM is used in the analysis of complex electronic packaging circuits printed on single or multilayer substrates. A typical microstrip discontinuity is illustrated in Fig. 1. The input port of the structure is excited using the dominant field distribution at a specific frequency. The governing field distribution at the input port is evaluated *a priori* using a 2-D eigenvalue analysis [14]. The input and output ports are appropriately terminated using ABC's that are directly applied to the transverse electric-field component at the surface. The same type of ABC's are also used to effectively terminate the sidewalls of open structures.

Although the 2-D analysis assumes that the surrounding walls are either perfect electric conducting (PEC) or perfect magnetic conducting (PMC) surfaces, the obtained solution may still be used as a proper excitation for open structures provided that the terminating sidewalls are placed far enough to allow decay of the evanescent fields along the transverse direction. Because of the highly attenuating nature of these fields, the error caused by the terminating sidewalls is basically negligible if the distance between the transmission line and mesh truncation is comparable to the distance between present discontinuities and ABC surfaces. Besides, implementation of boundary conditions for evanescent fields in an eigenvalue analysis, although straightforward, requires knowledge of the precise attenuation rate of the fields along the transverse direction. The corresponding attenuation constant is geometry specific and is usually estimated based on approximate empirical formulas [18].

The 3-D finite-element analysis begins with the discretization of Helmholtz's equation in the following source-free region:

$$\nabla \times ([\mu_r]^{-1} \cdot \nabla \times \boldsymbol{E}) - k_\circ^2 [\epsilon_r] \boldsymbol{E} = 0 \tag{1}$$

where $[\epsilon_r]$ and $[\mu_r]$ are, respectively, the relative permittivity and permeability tensors of the domain. Using the well-known Galerkin's technique, the Helmholtz's equation may be transformed in a weak integral form given by

$$\begin{aligned}\int_\Omega ([\mu_r]^{-1} \nabla \times \boldsymbol{E}) \cdot (\nabla \times \boldsymbol{N})\, dV - k_\circ^2 \int_\Omega [\epsilon_r] \cdot \boldsymbol{E} \cdot \boldsymbol{N}\, dV \\ + \int_{S_1} ([\mu_r]^{-1} \nabla \times \boldsymbol{E}) \cdot (\boldsymbol{N} \times \hat{a}_n)\, dA \\ + \int_{S_2} ([\mu_r]^{-1} \nabla \times \boldsymbol{E}) \cdot (\boldsymbol{N} \times \hat{a}_n)\, dA \\ + \int_{S_3} ([\mu_r]^{-1} \nabla \times \boldsymbol{E}) \cdot (\boldsymbol{N} \times \hat{a}_n)\, dA = 0\end{aligned} \tag{2}$$

where S_1 and S_2 denote the input and output ports, respectively, whereas S_3 denotes all open wall surfaces. The unit vector $\hat{a}_n$ is normal to a given surface and is pointing outside the finite-element volume, whereas $\boldsymbol{N}$ is the vector testing function. To evaluate the surface integrals in (2), appropriate boundary conditions need to be developed at those surfaces [11], [15]. The development of such boundary conditions mandates expressing the electric field on the surface in terms of the transverse and longitudinal components, designated by the subscripts t and n as follows:

$$\boldsymbol{E} = \boldsymbol{E}_t + \hat{a}_n E_n. \tag{3}$$

The normal component of the electric field E_n is further assumed to be negligible. This assumption is implemented only in the evaluation of the surface integrals. As a result, the total electric field at the excitation plane can be expressed as a superposition of two transverse field components, i.e.,

$$\boldsymbol{E}(x,y,z) \simeq \boldsymbol{E}_t(x,y,z) = \boldsymbol{E}_t^{\text{inc}}(x,y,z) + \boldsymbol{E}_t^{\text{sca}}(x,y,z) \tag{4}$$

where the superscripts inc and sca denote incident and scattered fields, respectively. The incident field in (4) is obtained from the 2-D eigenvalue analysis, i.e.,

$$\boldsymbol{E}_t^{\text{inc}}(x,y,z) = E_\circ \boldsymbol{e}_t(x,y) e^{-jk_z z} \tag{5}$$

where $\boldsymbol{e}_t(x,y)$ is the field distribution of the dominant mode at the input port and k_z is the corresponding propagation constant. Expressing the incident field in the form shown in (5), it was assumed that the input port lies on the xy-plane. Substituting (5) into (4), the total transverse field at the input port is represented as

$$\begin{aligned}\boldsymbol{E}(x,y,z) &\simeq \boldsymbol{E}_t(x,y,z) \\ &= E_\circ \boldsymbol{e}_t(x,y) e^{-jk_z z} + R E_\circ \boldsymbol{e}_t(x,y) e^{jk_z z}\end{aligned} \tag{6}$$

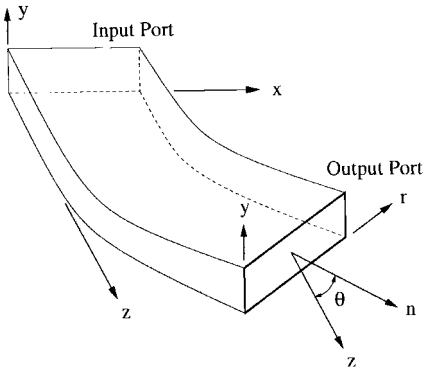

Fig. 2. Two-port geometry with the output port oriented at an angle θ with respect to the input port.

where R is the reflection coefficient. Based on (6), the following first-order ABC is valid [11]:

$$-\hat{a}_z \times (\nabla \times \boldsymbol{E}) + jk_z \hat{a}_z \times (\hat{a}_z \times \boldsymbol{E}) = -2jk_z \boldsymbol{E}^{\text{inc}}. \quad (7)$$

A similar ABC can be derived for the output port as well. The planar surface of the output port lies on the ry-plane where $\hat{a}_r \times \hat{a}_y$ forms a unit vector normal to the port plane. This unit vector forms an angle θ with respect to the unit vector $\hat{a}_z$. In other words, the output port plane does not have to be parallel with the input port plane (see Fig. 2). As a result, geometries such as waveguide and microstrip bends may be analyzed.

Referring to Fig. 2, the total field at the output port can be expressed in the following form:

$$\boldsymbol{E}(x,y,z) \simeq \boldsymbol{E}_t(x,y,z) = TE_\circ \boldsymbol{e}_t(r,y) e^{-jk_n(x\sin\theta + z\cos\theta)} \quad (8)$$

where T is the transmission coefficient and k_n is the effective propagation constant in the direction represented by

$$\hat{n} = \hat{a}_x \sin\theta + \hat{a}_z \cos\theta. \quad (9)$$

Based on the orientation of the output port and the corresponding field distribution at that plane, a valid first-order ABC is given by [11]

$$\hat{a}_n \times (\nabla \times \boldsymbol{E}) + jk_n \hat{a}_n \times (\hat{a}_n \times \boldsymbol{E}) = 0. \quad (10)$$

Substituting (7) and (10) into (2), the latter becomes

$$\begin{aligned}\int_\Omega ([\mu_r]^{-1} \nabla \times \boldsymbol{E}) \cdot (\nabla \times \boldsymbol{N})\, dV - k_\circ^2 \int_\Omega [\epsilon_r] \cdot \boldsymbol{E} \cdot \boldsymbol{N}\, dV \\ + jk_z \int_{S_1} ([\mu_r]^{-1} \boldsymbol{E} \times \hat{a}_{n_1}) \cdot (\boldsymbol{N} \times \hat{a}_{n_1})\, dA \\ + jk_n \int_{S_2} ([\mu_r]^{-1} \boldsymbol{E} \times \hat{a}_{n_2}) \cdot (\boldsymbol{N} \times \hat{a}_{n_2})\, dA \\ + \int_{S_3} ([\mu_r]^{-1} \nabla \times \boldsymbol{E}) \cdot (\boldsymbol{N} \times \hat{a}_{n_3})\, dA \\ = -2jk_z \int_{S_1} ([\mu_r]^{-1} \boldsymbol{E}_t^{\text{inc}} \times \hat{a}_{n_1}) \cdot (\boldsymbol{N} \times \hat{a}_{n_1})\, dA \quad (11)\end{aligned}$$

where $\hat{a}_{n_1} = -\hat{a}_z, \hat{a}_{n_2} = \hat{a}_x \sin\theta + \hat{a}_z \cos\theta$, and $\hat{a}_{n_3}$ is the outward unit vector normal to the open wall surfaces. The ABC at the open walls is very similar to the one implemented at the output port. The only difference between the two is that k_n is replaced by $k_\circ \sqrt{\epsilon_r \mu_r}$ where ϵ_r and μ_r are, respectively, the permittivity and permeability of the local medium. By introducing tetrahedral elements, the electric field $\boldsymbol{E}$ is expanded in terms of a set of vector basis functions $\boldsymbol{N}$ to finally obtain the following elemental matrix system:

$$[M^e + B^e_{S_1} + B^e_{S_2} + B^e_{S_3}]\{E^e\} = \{b^e\} \quad (12)$$

where

$$\begin{aligned}M^e(i,j) = \int_{\Omega^e} \{\nabla \times \boldsymbol{N}_i\}^T \cdot [\mu_r]^{-1} \cdot \{\nabla \times \boldsymbol{N}_j\}\, dV \\ - k_\circ^2 \int_{\Omega^e} \boldsymbol{N}_i^T \cdot [\epsilon_r] \cdot \boldsymbol{N}_j\, dV \quad (13)\end{aligned}$$

$$\begin{aligned}B^e_{S_1}(i,j) = jk_z \int_{S_1^e} \{\boldsymbol{N}_i \times \hat{a}_{n_1}\}^T \cdot [\mu_r]^{-1} \\ \cdot \{\boldsymbol{N}_j \times \hat{a}_{n_1}\}\, dA \quad (14)\end{aligned}$$

$$\begin{aligned}B^e_{S_2}(i,j) = jk_n \int_{S_2^e} \{\boldsymbol{N}_i \times \hat{a}_{n_2}\}^T \cdot [\mu_r]^{-1} \\ \cdot \{\boldsymbol{N}_j \times \hat{a}_{n_2}\}\, dA \quad (15)\end{aligned}$$

$$\begin{aligned}B^e_{S_3}(i,j) = jk_\circ \sqrt{\epsilon_r \mu_r} \int_{S_3^e} \{\boldsymbol{N}_i \times \hat{a}_{n_3}\}^T \cdot [\mu_r]^{-1} \\ \cdot \{\boldsymbol{N}_j \times \hat{a}_{n_3}\}\, dA \quad (16)\end{aligned}$$

$$\begin{aligned}b^e(i) = -2jk_z \int_{S_1^e} \{\boldsymbol{N}_i \times \hat{a}_{n_1}\}^T \cdot [\mu_r]^{-1} \\ \cdot \{\boldsymbol{E}_t^{\text{inc}} \times \hat{a}_{n_1}\}\, dA \quad (17)\end{aligned}$$

where $i,j = 1,\cdots,6$. The elemental matrices are then assembled into the global matrix using the edge connectivity information. The global matrix system is solved using an efficient conjugate gradient-square (CGS) solver with Jacobi preconditioning. For better and faster convergence, the iteration is done in double precision.

Once the electric-field distribution is obtained everywhere in the structure, the next step is to evaluate the corresponding voltages at the two ports. Note that although the theoretical formulation was based on a two-port network, it can be easily extended for multiple ports. The S-parameters of the structure are evaluated using

$$S_{11} = \frac{V_1 - V_1^{\text{ref}}}{V_1^{\text{ref}}} \quad (18)$$

$$S_{21} = \frac{V_2}{V_1^{\text{ref}}} \sqrt{\frac{Z_{c1}}{Z_{c2}}} \quad (19)$$

where V_1 and V_2 are the voltages calculated at ports 1 and 2 (3-D analysis), respectively, whereas V_1^{ref} is the reference voltage calculated at port 1 (2-D analysis). Also, Z_{c1} and Z_{c2} are the corresponding characteristic impedances of the transmission lines at the two ports. These are calculated using the 2-D finite-element eigenvalue analysis.

III. The FDTD Method

The FDTD method is one of the most popular numerical techniques for solving complex electromagnetic problems. The FDTD method is finding applications in a wide spectrum of simulation problems including antennas for wireless communications, biomedical applications, microwave circuits,

electronic packaging, and electromagnetic scattering and penetration. The popularity of this method is attributed to its simplicity in implementation and computer programming, its ability to handle arbitrary and complex geometries including different materials, and the fact that it is a time-domain method.

An FDTD code suitable for handling general multiconductor structures has been developed. The code is quite general in handling different material and conductor discontinuities, such as the ones found in electronic packages. The developed code uses first-order Mur ABC's. These have been proven to work well in applications involving microwave circuits. The electric-wall source condition has been implemented to excite the dominant mode of structures investigated in this paper. Since the FDTD method uses rectangular bricks as the basic mesh elements, it is predominantly suited for planar structures. For structures characterized by curved surfaces, the FEM is more suitable.

In obtaining the S-parameters of a given structure, a source plane is imposed at the input port. The excitation signal is a Gaussian pulse in the time domain. Once the pulse is launched, the first-order Mur ABC's are immediately turned on. The numerical simulation is carried out twice. The first simulation occurs in the absence of the discontinuity. This is required in order to establish a reference incident waveform propagating along the microstrip line. The reference plane is defined N cells away from the beginning of the discontinuity. A second simulation is repeated in the presence of the discontinuity and the time signature of the incident and reflected voltages at the reference plane is obtained. Using the two simulations, the incident and reflected time-domain waveforms are first calculated and then used to evaluate the amplitude and phase of the return loss (RL). A similar argument holds for the transmitted voltage used in the evaluation of the insertion loss (IL) of the structure.

IV. Results

The finite-element formulation presented in Section II was successfully implemented and applied to a variety of circuits and interconnects that are frequently used in microwave electronic packages. The FEM was extensively verified by comparing it with results obtained using the FDTD method briefly outlined in Section III.

The first geometry considered, primarily for verification purposes, is a rectangular microstrip patch antenna, which is printed on a RT/Duroid substrate with $\epsilon_r = 2.2$ and height 0.794 mm. A 50-Ω microstrip line is used to excite the patch. The same exact geometry was analyzed by Sheen *et al.* [6] using the FDTD method. The mesh sizes suggested in [6] were also used here; i.e., $\Delta x = 0.389$ mm, $\Delta y = 0.4$ mm, $\Delta z = 0.265$ mm, and $\Delta t = 0.441$ ps. These mesh sizes result in an integral number of cells along the width and length of the patch, but not along the width of the microstrip line feeding the patch. The resulting FDTD mesh dimensions are $61 \times 100 \times 17$ cells.

A comparison of the RL obtained using the FEM and the FDTD method is shown in Fig. 3. A fairly good agreement between the two methods is illustrated. For frequencies lower than 10 GHz (where the mesh density is sufficiently fine), the agreement between the two numerical techniques is excellent. Two different finite-element discretizations were considered: one with 22 702 tetrahedras and the other with 28 883 tetrahedras. However, as shown in Fig. 3, only a minor improvement is observed in the predictions when running the larger discretization. A possible source of error in the calculations is the inability of the FDTD method to properly match all microstrip-surface dimensions. A narrower microstrip line for example, always results in a larger characteristic impedance, thereby affecting the RL of the structure, especially at the higher frequencies. On the other hand, using the FEM, all geometry dimensions are precisely modeled.

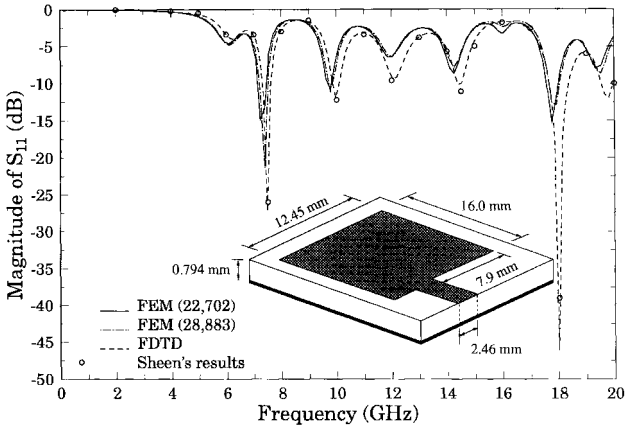

Fig. 3. Return loss of a rectangular microstrip patch antenna printed on a RT/Duroid substrate with $\epsilon_r = 2.2$.

In order to provide insight into the computational effort required by the FEM, the following statistics were reported. The original mesh consisted of 22 702 tetrahedras and a total of 25 625 unknowns. The computational time was approximately 30 min per frequency point in the lower frequency range and 15 min per frequency point in the upper frequency range. This problem was run on a 370 IBM RISC/6000 UNIX workstation. The solution tolerance based on the residual norm was set to $1.0e{-}6$. The recorded computational time also accounts for the central processing unit (CPU) time needed in evaluating the modal field distribution at the input port. On the other hand, the FDTD code took approximately 45 min for the overall simulation, and 8192 time steps were allowed for the pulse to propagate. The simulation was done on a Silicon Graphics Power Indigo2 workstation with an R8000 processor. Note that the latter is a significantly faster computer than the 370 IBM RISC/6000.

The second circuit considered in this paper was also extracted from Sheen *et al.* [6]. This is a low-pass filter which is printed on an RT/Duroid substrate with $\epsilon_r = 2.2$ and height 0.794 mm. This geometry was run using both the FEM and the FDTD codes for a frequency range of 20 GHz. The magnitude of S_{11} and S_{21} versus frequency is illustrated in Fig. 4. Excellent agreement between the two methods is shown. The finite-element mesh consisted of 28 914 tetrahedras and a total of 33 532 unknown field components. The corresponding CPU time for this problem was approximately

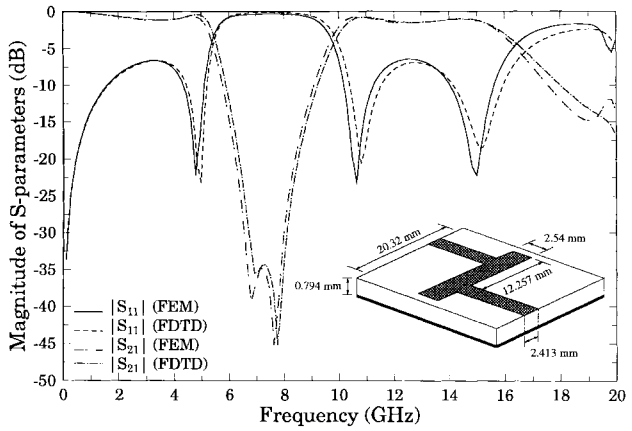

Fig. 4. Return and insertion loss of a low-pass filter printed on a RT/Duroid substrate with $\epsilon_r = 2.2$.

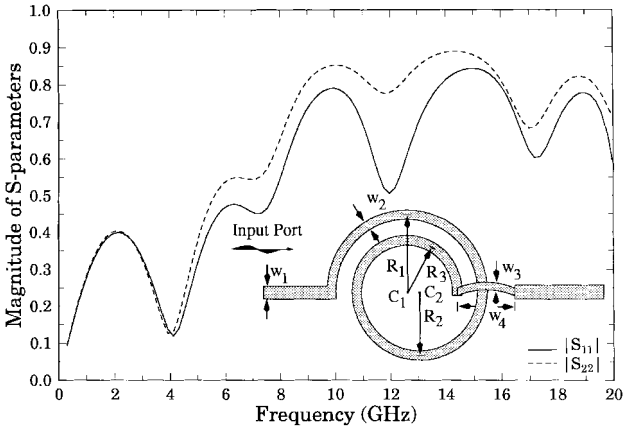

Fig. 5. S-parameters of a spiral inductor connected in series with two microstrip lines. The substrate is made of alumina of $\epsilon_r = 9.8$ and height 0.635 mm ($w_1 = 0.635$ mm, $w_2 = w_3 = 0.2$ mm, $w_4 = 2.3$ mm, $R_1 = 1.9$ mm, $R_2 = 1.3$ mm, $R_3 = 0.7$ mm).

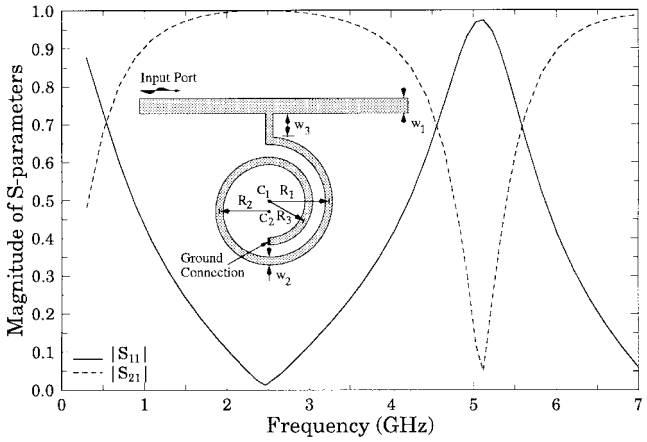

Fig. 6. S-parameters of a spiral inductor connected in shunt across a microstrip line. The substrate is made of alumina of $\epsilon_r = 9.8$ and height 0.635 mm ($w_1 = 0.635$ mm, $w_2 = 0.2$ mm, $w_3 = 0.6$ mm, $R_1 = 1.9$ mm, $R_2 = 1.3$ mm, $R_3 = 0.7$ mm).

20 min per frequency point in the lower frequency range and 10 min per frequency point in the upper frequency range. Note that although the low-pass filter is computationally a larger problem than the microstrip patch antenna, the required CPU time is significantly less. The reason is related to the condition number of the resulting matrix system. As far as the FDTD method is concerned, the mesh dimensions were the following: $\Delta x = 0.4064$ mm, $\Delta y = 0.4233$ mm, $\Delta z = 0.265$ mm, and $\Delta t = 0.441$ ps. The overall mesh size was $81 \times 101 \times 17$ cells. The required computational time was approximately 50 min, and again, a total of 8192 time steps were allowed for the pulse to propagate. The simulation was run on a Silicon Graphics Power Indigo2 workstation with an R8000 processor.

Although spiral inductors, as well as inductors in general, are commonly found in microwave circuits, most of the relevant analysis has been done based on either quasi-static methods [19] or rectangular-grid methods such as the FDTD, SDA, transmission-line method (TLM), and method of lines (MoL) [20]. Using the FEM, electromagnetic modeling of curved structures presents no more difficulties than rectangular structures provided that the code is written using unstructured elements. A circular spiral inductor connected in series with a microstrip line on an alumina substrate with $\epsilon_r = 9.8$ is considered here. One end of the spiral is bonded with the microstrip line at port 2 through a cylindrical metallic bridge. The bridge surface is defined by three points: the first point is in the center of the spiral, the second point is at the edge of the microstrip line, and the third point is in the middle of the gap (height of 1.0 mm). The spiral is made out of $1\frac{1}{2}$ turns with width 0.2 mm. The microstrip line at the input and output ports is 0.635-mm wide, and the substrate height is also 0.635 mm. The magnitude of S_{11} and S_{22} calculated using the FEM is illustrated in Fig. 5. Although measurements were not available for data comparison, the geometry discretization in both cases was sufficiently fine to ensure accurate simulations. Specifically, the mesh consisted of 27 701 elements and a total of 32 553 unknowns. The corresponding computational time was approximately 1 h per frequency point in the lower range of frequencies, and 20 min per frequency point in the intermediate-to-upper range of frequencies; again, a 370 IBM RISC/6000 workstation was used to run this problem. Most of the computational effort (90%) was spent solving the linear system of equations. Comparing the two plots in Fig. 5, it is interesting to observe that those are not identical, although very similar. The minor differences are basically attributed to the presence of the cylindrical metallic bridge. In addition, it is important to mention here that the spiral inductor behaves as a lumped element only in the lower range of frequencies (linear region); at higher frequencies, the structure begins to resonate due to additive capacitive effects.

A spiral inductor is usually connected either in series or in parallel. The same configuration as the one used in the previous example is now connected in shunt with a microstrip line printed on an alumina substrate. The center of the spiral is grounded using a planar conducting via. The magnitude plots of S_{11} and S_{21} calculated using the FEM code are shown in Fig. 6. Although comparisons are not available, it is interesting to observe that at lower frequencies the structure indeed behaves as a lumped inductor connected in shunt. Such a structure though is highly resonant; therefore, multiple peaks

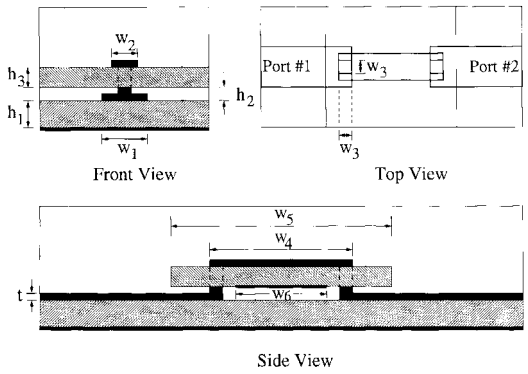

Fig. 7. Double-via-transition package. The bottom and top layers have dielectric constants of 2.2 and 6.2, respectively ($h_1 = 0.8$ mm, $h_2 = 0.4$ mm, $h_3 = 0.6$ mm, $w_1 = 2.4$ mm, $w_2 = 0.8$ mm, $w_3 = 0.4$ mm, $w_4 = 5.2$ mm, $w_5 = 6.8$ mm, $w_6 = 3.6$ mm, $t = 0.2$ mm).

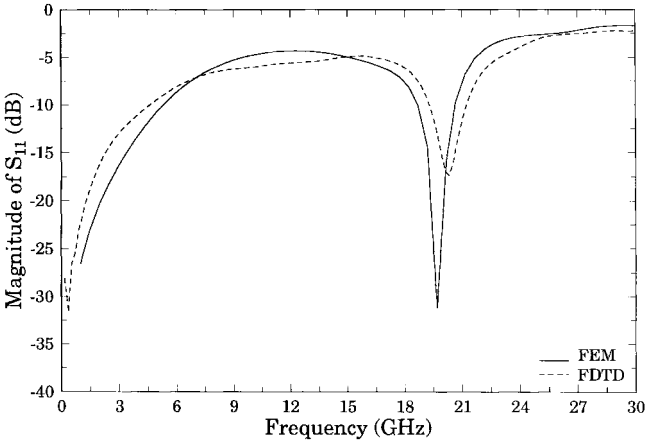

Fig. 8. S_{11} versus frequency for the double-via-transition package.

and nulls appear in the higher frequency range. As a result, the resulting S-parameters are plotted only up to 7 GHz. The finite element mesh for this problem consisted of 43 588 tetrahedras and a total of 51 270 unknowns.

The final structure examined is the two-layer package shown in Fig. 7, which is representative of practical designs. The bottom layer is a dielectric substrate with $\epsilon_r = 2.2$, whereas the top layer is another substrate with $\epsilon_r = 6.2$. The microstrip at the input port is connected to the microstrip at the upper layer through a vertical conducting via, and an identical via joins the upper microstrip with the microstrip at the output port. A metallic sheet is placed at the bottom interface of the upper dielectric layer to provide potential grounding. Also, all geometry shapes were chosen to be rectangular so the simulation is performed with both FEM and FDTD codes. The magnitude of S_{11} versus frequency, calculated using the two numerical techniques, is illustrated in Fig. 8. Although both methods accurately predict the resonant frequency of the package, there are some minor discrepancies between the two data sets. The reason might be attributed to nonphysical reflections from the surrounding first-order ABC's. More efficient mesh terminations, such as the recently developed perfectly matched layer (PML) [21]–[23] or other higher order ABC's, need to be implemented in both FEM and FDTD methods to further reduce possible truncation errors.

V. Conclusions

The FEM has been applied in the analysis of microwave electronic circuits and interconnects. The input port is excited using a 2-D eigenvalue solution, whereas all ports are terminated using first-order dispersive ABC's based on the effective dielectric constant. The open sidewalls are also terminated using first-order ABC's. For few of these geometries, a comparison with the FDTD method is provided. Obtained S-parameters illustrate good agreement between the two numerical techniques. Although the FEM is shown to be computationally more intensive than the FDTD method (at least for the cases considered in this paper), it exhibits numerous advantages over many numerical techniques—most importantly, the ability to accurately model curved surfaces and inhomogeneous materials, both of which are commonly employed in electronic packages and microwave circuits.

Acknowledgment

The authors would like to thank Dr. J. F. Harvey of the Electronics Division, Army Research Office (ARO), Research Triangle Park, NC, and Dr. J. W. Mink, formerly of ARO, for their interest and support of the project.

References

[1] K. S. Yee, "Numerical solution of initial boundary value problems in involving Maxwell's equations in isotropic media," *IEEE Trans. Antennas Propagat.*, vol. AP-14, pp. 302–307, May 1966.
[2] R. W. Jackson, "Full-wave, finite element analysis of irregular microstrip discontinuities," *IEEE Trans. Microwave Theory Tech.*, vol. 37, pp. 81–89, Jan. 1989.
[3] P. Silvester, "Finite element solution of homogeneous waveguide problems," *Alta Frequenza*, vol. 38, pp. 313–317, May 1989.
[4] X. Zhang and K. K. Mei, "Time-domain finite difference approach to the calculation of frequency-dependent characteristics of microstrip discontinuities," *IEEE Trans. Microwave Theory Tech.*, vol. 36, pp. 1775–1787, Dec. 1988.
[5] X. Zhang, J. Fang, K. K. Mei, and Y. Liu, "Calculations of the dispersive characteristics of microstrips by the time-domain finite difference method," *IEEE Trans. Microwave Theory Tech.*, vol. 36, pp. 263–267, Feb. 1988.
[6] D. M. Sheen, S. M. Ali, M. D. Abouzahra, and J. A. Kong, "Application of the three-dimensional finite-difference time-domain method to the analysis of planar microstrip circuits," *IEEE Trans. Microwave Theory Tech.*, vol. 38, pp. 849–857, July 1990.
[7] A. Christ and H. L. Hatnagel, "Three-dimensional finite-difference method for the analysis of microwave-device embedding," *IEEE Trans. Microwave Theory Tech.*, vol. MTT-35, pp. 688–696, Aug. 1987.
[8] T. Becks and I. Wolff, "Analysis of 3-D metallization structures by a full-wave spectral domain technique," *IEEE Trans. Microwave Theory Tech.*, vol. 40, pp. 2219–2227, Dec. 1992.
[9] J. C. Nedelec, "Mixed finite elements in R^3," *Numer. Math.*, vol. 35, pp. 315–341, 1980.
[10] A. F. Peterson, "Absorbing boundary conditions for the vector wave equation," *Microwave Opt. Techol. Lett.*, vol. 1, pp. 62–64, Apr. 1988.
[11] J. Jin, *The Finite Element Method in Electromagnetics*. New York: Wiley, 1993.
[12] K. Ise, K. Inoue, and M. Koshiba, "Three-dimensional finite-element method with edge elements for electromagnetic waveguide discontinuities," *IEEE Trans. Microwave Theory Tech.*, vol. 39, pp. 1289–1295, Aug. 1991.
[13] J.-F. Lee, D. Sun, and Z. J. Cendes, "Full-wave analysis of dielectric waveguides using tangential vector finite elements," *IEEE Trans. Microwave Theory Tech.*, vol. 39, pp. 1262–1271, Aug. 1991.

[14] A. C. Polycarpou, M. R. Lyons, and C. A. Balanis, "Finite element analysis of MMIC waveguide structures with anisotropic substrates," *IEEE Trans. Microwave Theory Tech.*, vol. 44, pp. 1650–1663, Oct. 1996.
[15] J.-S. Wang and R. Mittra, "Finite element analysis of MMIC structures and electronic packages using absorbing boundary conditions," *IEEE Trans. Microwave Theory Tech.*, vol. 42, pp. 441–449, Mar. 1994.
[16] _____, "A finite element cavity resonance method for waveguide and microstrip line discontinuity problems," *IEEE Trans. Microwave Theory Tech.*, vol. 42, pp. 433–440, Mar. 1994.
[17] J.-G. Yook, D. I. Nihad, and L. P. B. Katehi, "Characterization of high frequency interconnects using finite difference time domain and finite element methods," *IEEE Trans. Microwave Theory Tech.*, vol. 42, pp. 1727–1736, Sept. 1994.
[18] J. Tan and G. Pan, "A new edge element analysis of dispersive waveguiding structures," *IEEE Trans. Microwave Theory Tech.*, vol. 43, pp. 2600–2607, Nov. 1995.
[19] E. Pettenpaul, H. Kapusta, A. Weisgerber, H. Mampe, J. Luginsland, and I. Wolff, "CAD models of lumped elements on GaAs up to 18 GHz," *IEEE Trans. Microwave Theory Tech.*, vol. 36, pp. 294–304, Feb. 1988.
[20] L. Vietzorreck and R. Pregla, "Hybrid analysis of three-dimensional MMIC elements by the method of lines," *IEEE Trans. Microwave Theory Tech.*, vol. 44, pp. 2580–2586, Dec. 1996.
[21] J. P. Berenger, "A perfectly matched layer for the absorption of electromagnetic waves," *J. Comput. Phys.*, vol. 114, no. 2, pp. 185–200, Oct. 1994.
[22] Z. S. Sacks, D. M. Kingsland, R. Lee, and J.-F. Lee, "A perfectly matched anisotropic absorber for use as an absorbing boundary condition," *IEEE Trans. Antennas Propagat.*, vol. 43, pp. 1460–1463, Dec. 1995.
[23] A. C. Polycarpou, M. R. Lyons, and C. A. Balanis, "A two-dimensional finite element formulation of the perfectly matched layer," *IEEE Microwave Guided Wave Lett.*, vol. 6, pp. 338–340, Sept. 1996.

Anastasis C. Polycarpou was born in Nicosia, Cyprus, in October 1967. He received the B.S. and M.S. degrees in electrical engineering (*summa cum laude*) from Arizona State University, Tempe, in 1992, and 1994, respectively, and is currently working toward the Ph.D. degree..

His research interests include analytical and computational electromagnetics in areas of electronic packaging, scattering, and antenna radiation.

Panayiotis A. Tirkas (S'89–M'92) was born in Nicosia, Cyprus. He received the B.S. and M.S. degrees in electrical engineering from the University of Kansas, Lawrence, in 1987 and 1989, respectively, and the Ph.D. degree in electrical engineering from Arizona State University, Tempe, in 1993.

From 1993 to 1997, he was employed as an Assistant Research Engineer at the Telecommunications Research Center at Arizona State University, where he coordinated the advanced helicopter electromagnetics consortium and conducted research on propagation models for mobile satellite communications, high-intensity radiated field (HIRF) penetration in aircraft, and electrical characterization of electronic packages. He is currently an Engineering Specialist at Space Systems/Loral, Palo Alto, California, where he is involved in the analysis, design, and testing of satellite antenna feeds and RF circuits. His current interests include the application of finite-element and mode-matching methods for the analysis and design of satellite antenna feeds and RF payloads, and in multipactor testing of satellite antenna components.

Dr. Tirkas is a member of Tau Beta Pi and Sigma Xi. He was the recipient of a Fulbright Exchange Scholarship (1982–1987), and an Aileen S. Andrew Foundation Fellowship (1989–1993).

Constantine A. Balanis (S'62–M'65–SM'74–F'86) received the B.S.E.E. degree from Virginia Polytechnic Institute and State University, Blacksburg, VA, in 1964, the M.E.E. degree from the University of Virginia, Charlottesville, in 1966, and the Ph.D. degree in electrical engineering from Ohio State University, Columbus, in 1969.

From 1964 to 1970, he was with NASA Langley Research Center, Hampton VA. From 1970 to 1983, he was with the Department of Electrical Engineering, West Virginia University, Morgantown. Since 1983, he has been with the Department of Electrical Engineering, Arizona State University, Tempe, where he is currently Regent Professor and Director of the Telecommunications Research Center. He is the author of *Antenna Theory: Analysis and Design* (Wiley, 1997, 1982) and *Advanced Engineering Electromagnetics* (Wiley, 1989). His research interests are in low- and high-frequency computational methods for antennas, scattering and penetration, transient analysis, control of coupling and reduction of pulse distortion in interconnects for monolithic microwave and millimeter-wave circuits, modeling of electronic packages for microwave, millimeter-wave, and high-speed high-density integrated circuits, and multipath propagation.

Dr. Balanis is a member of ASEE, Sigma Xi, Electromagnetics Academy, Tau Beta Pi, Eta Kappa Nu, and Phi Kappa Phi. He received the 1992 Special Professionalism Award from the IEEE Phoenix Section in 1992, the IEEE Region 6 Individual Achievement Award in 1989, the Arizona State University Outstanding Graduate Mentor Award in 1996, and the 1987–1988 Graduate Teaching Excellence Award, School of Engineering, Arizona State University. He has served as associate editor of the IEEE TRANSACTIONS ON ANTENNAS AND PROPAGATION (1974–1977) and the IEEE TRANSACTIONS ON GEOSCIENCE AND REMOTE SENSING (1981–1984), and as editor of the IEEE Geoscience and Remote Sensing Society (1982–1983) Newsletter. He has served as second vice-president (1984) and member of the administrative committee (1984–85) of the IEEE Geoscience and Remote Sensing Society, and as chairman of the Distinguished Lecturer Program of the IEEE Antennas and Propagation Society (1988–1991) and is member of the AdCom (1992–1995, 1997–1999) of the IEEE Antennas and Propagation Society.